scientific reports

Check for updates

OPEN

Unraveling the diversity of Arc volcanism and deep low-frequency tremors in Southwest Japan from numerical modeling

Goeun Ha[1,2], Changyeol Lee[3]✉ & YoungHee Kim[1,2]✉

Differences in slab dehydration and fluid transport influence the distribution of magmatism and deep low-frequency tremors in subduction zones. Southwest Japan, particularly Kyushu and Shikoku/Chugoku, exhibits significant along-arc variation in the spatial distribution of Quaternary arc volcanoes and adakites as well as deep low-frequency tremors beneath the forearc. Using two-dimensional numerical modeling, we quantitatively evaluate melting and fluid transport via a weak hydrous layer on the slab interface since the subduction initiation to clarify the observed key differences. In Kyushu, our model shows that dehydration of the colder subducting slab is mostly completed at sub-arc depths of 80–120 km, triggering intense flux melting in the mantle wedge and an absence of sub-forearc fluid percolation for the tremors. Adakitic signature in Kyushu could be diluted by the basaltic magma in the mantle wedge which the adakitic magma traverses. Whereas the model for Shikoku/Chugoku shows shallower sub-forearc dehydration of the warmer slab (< 80 km), allowing less flux melting, slab melting for adakite, and sub-forearc fluid percolation for the tremors.

In subduction zones, fluid (e.g., H_2O and CO_2) expelled from the subducting oceanic lithosphere via dehydration percolates through the slab itself and overlying mantle wedge, causing distinctive magmatic and seismic activities. Fluid-induced partial melting in the mantle wedge can be accompanied by melting of the subducting oceanic crust, resulting in a volcanic arc that includes adakites[1–4]. Simultaneously, a weak hydrous layer is formed on the sub-forearc slab interface via mantle hydration (e.g., serpentinization), which mechanically decouples the slab from the overlying forearc mantle, creating a cold and stagnant forearc mantle that extends to depths of 70 to 80 km[5–7]. The fluid flow toward the mantle wedge corner through the weak hydrous layer causes fault instability along the subduction thrust and triggers deep low-frequency tremors beneath the forearc[8]. The deep low-frequency tremors have been identified in Southwest Japan at depths of 30–40 km along the slab interface, exhibiting an along-arc distribution[9–11].

The dehydration/hydration, partial melting, and fluid behavior within the mantle wedge and slab are primarily governed by pressure and temperature, which closely correlate with the subduction parameters of the plate, including its age, dip, and convergence rate[12–14]. Among various subduction zones, the Southwest (SW) Japan subduction zone formed by the sinking of the Philippine Sea Plate (PHS) since ~ 17 Ma is a natural laboratory that exhibits distinct along-trench variations in subduction parameters[15] (Fig. 1). Compared to the convergence rate, the age and dip of the downgoing plate significantly vary along the trench; the older (colder) slab (> 50 Ma) subducts steeply beneath Kyushu, whereas the younger (warmer) slab aged between 15 and 25 Ma gently subducts beneath Shikoku/Chugoku[16,17]. This along-trench variation in slab age and dip may account for the uneven distribution of volcanic and seismic activities in a single subduction zone.

Kyushu exhibits active and dense arc volcanism, whereas Shikoku/Chugoku features only four monogenic Quaternary arc volcanoes, located farther from the trench (Fig. 1). Supporting this spatial variation, anomalously high Sr/Y ratios, a geochemical signature of adakitic magma, are only observed in the Sanbe and Daisen volcanoes in Chugoku[3] (Fig. 1). Despite these differences, trench-parallel fast directions of shear wave splitting are observed in the forearc of both regions, indicating the presence of serpentinites in the weak hydrous layer[18,19]. However, a belt-like distribution of deep low-frequency tremors is only present along the forearc in Shikoku[9]

[1]Center for Deep-Surface Coupling of Earth, Seoul National University, 1 Gwanak–ro, Gwanak–gu, Seoul 08826, Republic of Korea. [2]School of Earth and Environmental Sciences, Seoul National University, 1 Gwanak–ro, Gwanak–gu, Seoul 08826, Republic of Korea. [3]Department of Earth System Sciences, Yonsei University, 50 Yonsei–ro Seodaemun–gu, Seoul 03722, Republic of Korea. ✉email: changyeol.lee@yonsei.ac.kr; younghkim@snu.ac.kr

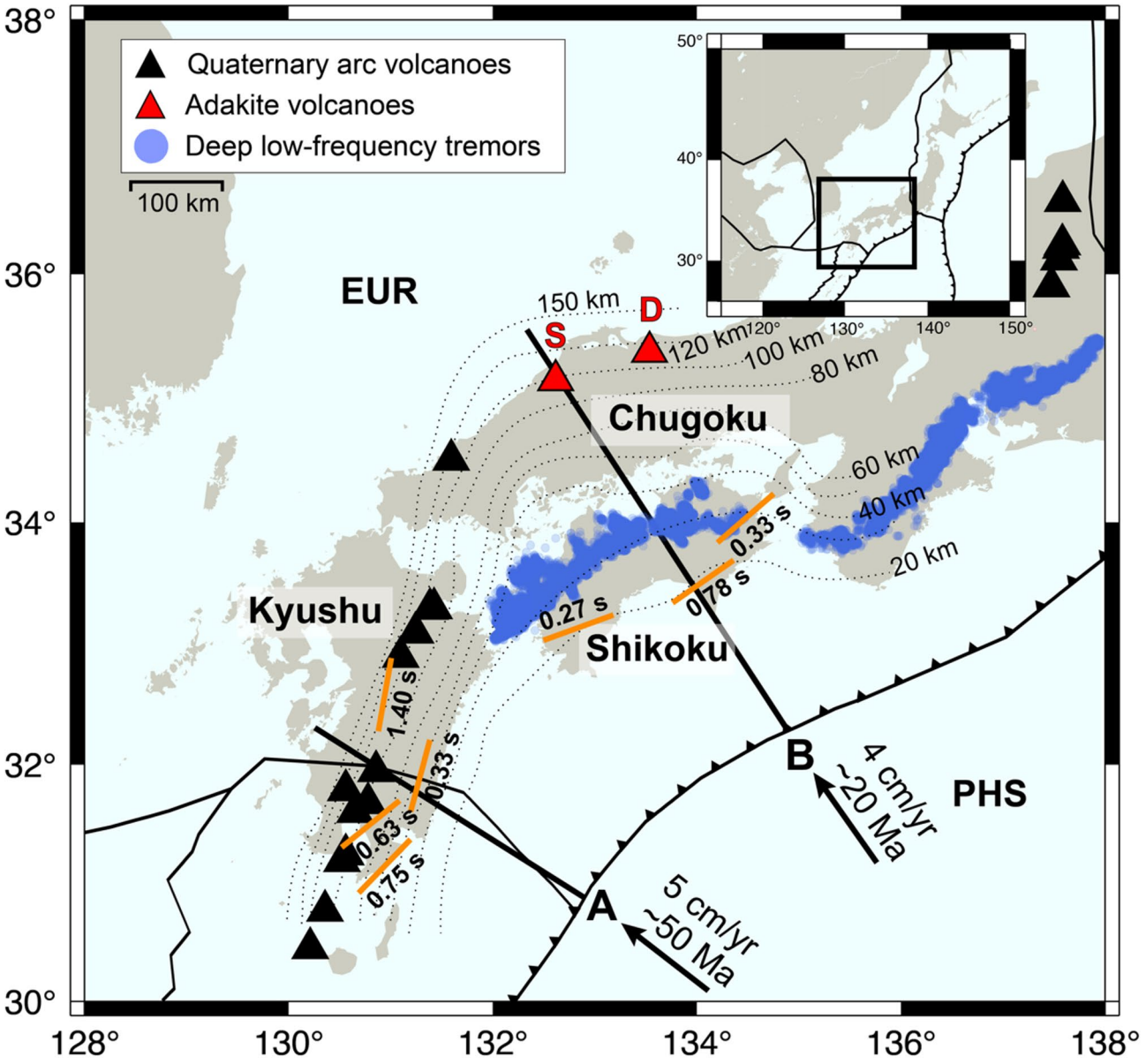

Fig. 1. A map of the Southwest (SW) Japan subduction zone showing geological and seismological observations. The Philippine Sea Plate (PHS) subducts beneath the Eurasian Plate (EUR) along the Nankai Trough represented by the barbed black lines[23]. Thin dotted lines denote depth contours of the upper boundary of the subducting PHS[24]. Black triangles show the Quaternary arc volcanoes in SW Japan; the Quaternary adakites are observed in the Sanbe (S) and Daisen (D) volcanoes. Blue open circles show the distribution of deep low-frequency tremors[25–28]; orange bars with texts below indicate fast polarization directions and delay time of S wave[19,29]. Model geometries of Kyushu and Shikoku/Chugoku are taken from profiles A and B, respectively. A map was adopted under CC BY-NC 4.0 from Fig. 1[ref.21] using the Generic Mapping Tools (https://generic-mapping-tools.org).

(Fig. 1), suggesting a regionally distinct pattern of fluid transport. This contrast likely reflects differences in slab thermal structure, controlled by along-trench variations in slab age and dip beneath the two regions.

Previous numerical model studies have attributed the contrasting spatial distributions of Quaternary volcanoes and deep low-frequency tremors in SW Japan to variations in slab dehydration, which are controlled by the thermal structure of the subducting slab and mantle wedge[17,20]. However, the prescribed (ad hoc) slab-mantle decoupling in previous models precludes the formation of a sub-forearc hydrous layer, which is essential for the seismic anisotropy and deep low-frequency tremors observed in the forearc. A recent modeling approach has provided important insights into how mechanical decoupling develops over time along the slab interface without a predefined slab-mantle decoupling zone[21]. The self-consistent dynamic decoupling by the downdip growth of the weak hydrous layer forms the cold stagnant forearc mantle (i.e., cold nose) through the transition from subduction infancy to mature subduction in SW Japan[21]as evidenced by the migration of the forearc-to-

arc volcanic front[22]. The study also shows that the presence of the weak hydrous layer and fluid percolation through the layer elucidates the volcanic and seismic activities in Shikoku/Chugoku. However, the study only targeted Shikoku/Chugoku, so it cannot explain the regional differences between the observations in Kyushu and Shikoku/Chugoku. Therefore, adopting their two-dimensional modeling framework, we capture geodynamical processes in Kyushu and Shikoku/Chugoku to understand the along-arc variations in volcanic and seismic activities observed in SW Japan.

Results

The model results for Kyushu and Shikoku/Chugoku show the formation and progressive growth of a weak hydrous layer induced by slab dehydration throughout the subduction evolution. During the early stages of subduction (i.e., 5 Myr after subduction initiation), a weak hydrous layer was developed near the wedge tip due to forearc hydration (Supplementary Figs. 1 and 2). The thermal anomaly observed in the slab beneath Shikoku/Chugoku resulted from the rapid subduction of a warm slab that has not had sufficient time to cool prior to subduction. The downdip extent of the weak hydrous layer progressively deepened over time, reaching approximately a depth of 90 km at present (Supplementary Figs. 3 and 4; Fig. 2). As the weak hydrous layer formed, the viscosity along the slab interface decreased by four to six orders of magnitude relative to the surrounding mantle, thereby facilitating the mechanical decoupling (Supplementary Figs. 5 and 6). This illustrates the transition of the slab interface from strong coupling to decoupling, resulting in the formation of a cold forearc mantle, as indicated by the modeled surface heat flow, slab surface temperature, and temperature of the mantle wedge beneath the arc (Supplementary Figs. 7, 8, and 9). The dehydration/hydration process occurring at depths greater than the sub-forearc shows different patterns depending on the slab temperature.

As the colder and steeper slab subducts in Kyushu at present, the slab temperature remains relatively low compared to that of Shikoku/Chugoku where the warmer and gentler slab subducts (Fig. 2a1 vs. 2a2). In Kyushu, the dehydration of the downgoing slab primarily occurred at sub-arc depths due to the lower temperatures. The basaltic and gabbroic oceanic crusts underwent continuous dehydration, which was almost completed by a depth of ~ 90 km, while the lithospheric mantle dehydrated at a depth of ~ 115 km (Figs. 2b1-2c1). The fluid

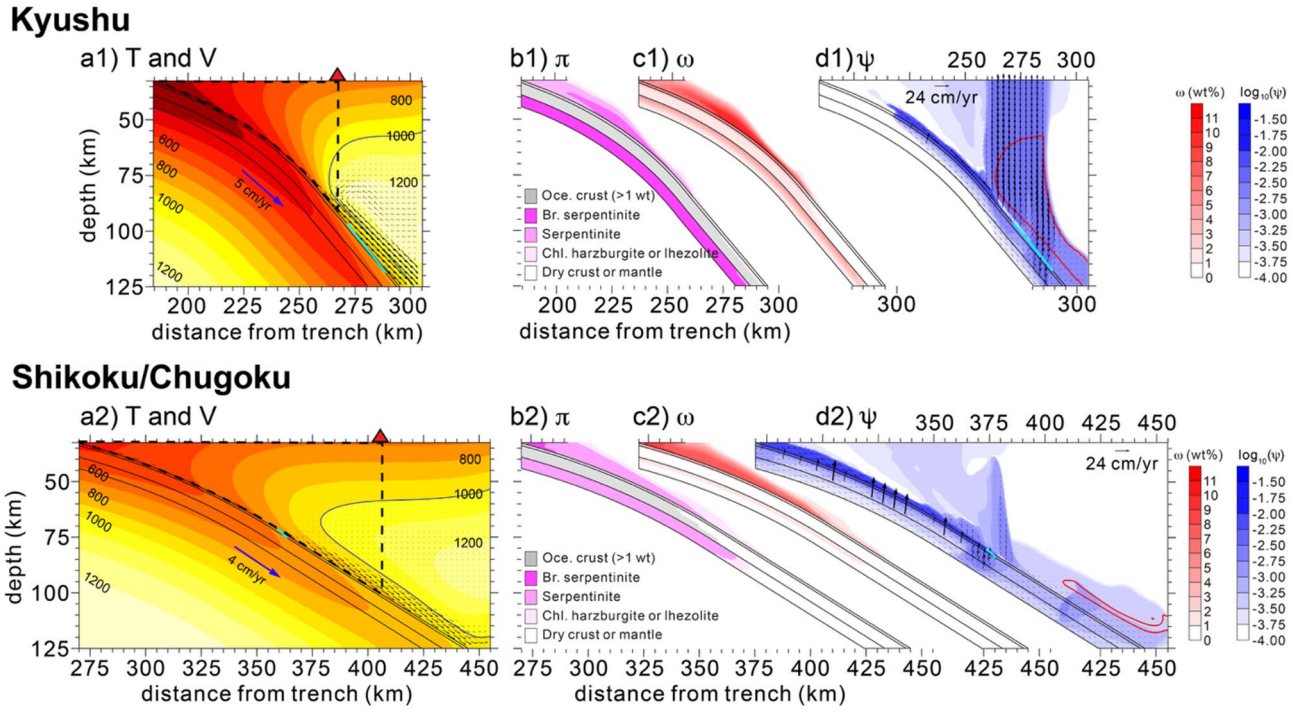

Fig. 2. Model results for Kyushu (a1-d1) and Shikoku/Chugoku (a2-d2) at present (0 Ma). (a1-a2) Distributions of temperature (T) and velocity (V). Black lines in the subducting plate indicate boundaries of the basaltic oceanic crust, gabbroic oceanic crust, and the hydrated portion of the lithospheric mantle. Red triangle indicates the location of arc volcano and the region enclosed by the black dashed line indicates the sub-forearc mantle wedge. The cyan line in the basaltic oceanic crust indicates the wet basalt solidus (750 °C). The thick blue contour in the mantle wedge represents the 1000 °C isotherm. (b1-b2) Distributions of major hydrous mineral phases (π) (e.g., Br. serpentinite (brucite-bearing serpentinite), serpentinite, and Chl. harzburgite or lherzolite (chlorite-bearing harzburgite or lherzolite) in the lithospheric mantle and mantle wedge. (c1-c2) Distributions of bound water (ω) in the crust, lithospheric mantle, and mantle wedge. (d1-d2) Distributions of free water (ψ) in the oceanic crust, hydrated lithospheric mantle, and mantle wedge. The fluid velocity is shown by black arrows. The red contour in the mantle wedge represents the potential flux melting zone (bound water > 0.1 wt% and T > 1000°C[ref.30]).

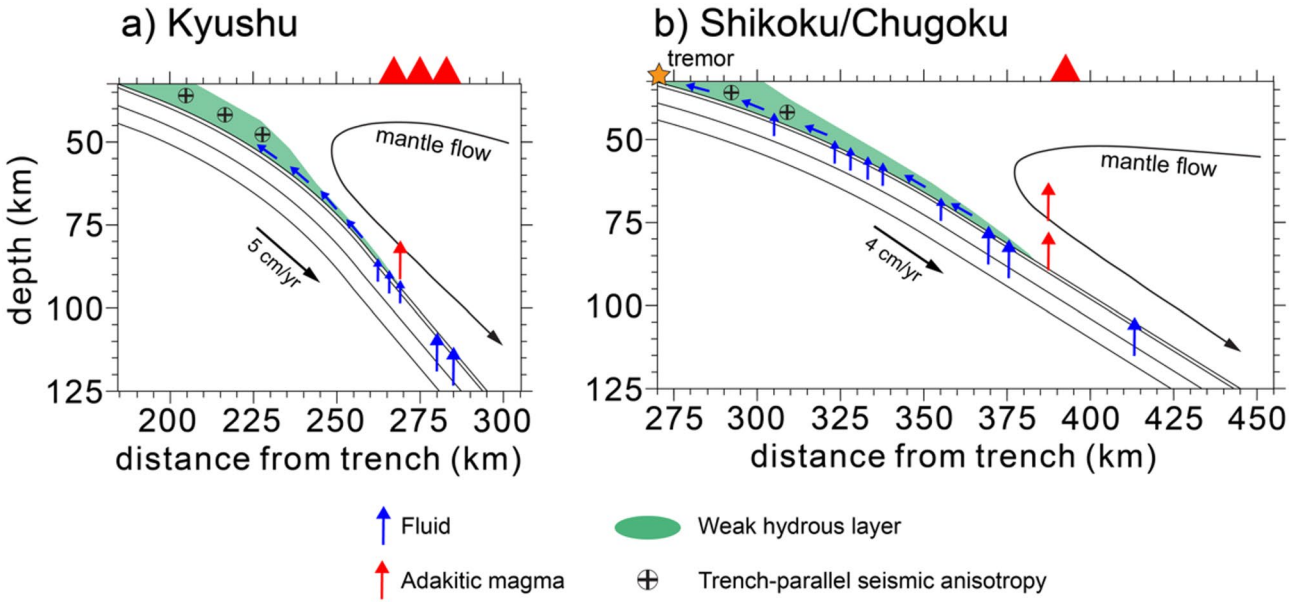

Fig. 3. Schematic descriptions of the geophysical and geochemical observations and the presence of the weak hydrous layer at the slab interface in (a) Kyushu and (b) Shikoku/Chugoku. The blue and red arrows indicate flow directions of the fluid and partial melt, respectively. The green shaded area represents the weak hydrous layer at the slab interface. In Kyushu, most fluid percolated to the mantle wedge at sub-arc depths, triggering flux melting. Only a small amount of fluid percolated along the weak hydrous layer and, consequently, did not reach the mantle wedge tip. In Shikoku/Chugoku, most fluid expelled at shallow depths percolated through the weak hydrous layer and reached the mantle wedge tip, generating deep low-frequency tremors. Only a small amount of fluid entered the overlying mantle, allowing less dilution between the basaltic magma by flux melting and adakitic magma by slab melting.

released by the breakdowns of the brucite-bearing serpentinite in the lithospheric mantle triggered flux melting in the overlying mantle wedge (bound water > 0.1 wt% and T > 1000°C[ref.30]; Fig. 2b1 and 2d1). The saturation of the fully dehydrated basaltic crust by the fluid supplied from the underlying lithospheric mantle led to slab melting at depths of 95–120 km, where temperatures exceeded the solidus of wet basalt (T > 750°C[ref.31]; Fig. 2d1). At its downdip extent of ~ 90 km, the lower portion of the weak hydrous layer released fluid into the sub-arc mantle wedge through the mineral breakdowns of the chlorite-bearing mantle (Figs. 2b1-2d1). Consequently, most of the fluid dehydrated from the oceanic crust and lithospheric mantle was supplied to the sub-arc mantle wedge, triggering flux melting. A small amount of fluid released from the downdip extent of the weak hydrous layer was supplied to the sub-forearc, but it did not reach the mantle wedge tip in Kyushu (Figs. 2b1-2d1).

In Shikoku/Chugoku, the percolation of slab-derived fluid was concentrated in the sub-forearc mantle wedge due to shallow dehydration and fluid migration toward the mantle wedge tip. The dehydration of the basaltic and gabbroic oceanic crusts continuously occurred until depths of less than 60 km and 25 km, respectively (Figs. 2b2-2c2). The breakdown of serpentinite in the lithospheric mantle released fluid at a depth of ~ 85 km, while the breakdown of brucite-bearing serpentinite was completed at depths shallower than 25 km (Figs. 2b2-2d2). The partial melting of the saturated basaltic crust by the expelled fluid from the underlying mantle occurred at depths of ~ 75 km[(e.g.,ref.32)] (Fig. 2d2). The mineral breakdowns of the lower portion of the weak hydrous layer supplied fluid to the sub-arc mantle wedge at its downdip extent of ~ 85 km (Figs. 2b2-2d2). Unlike in Kyushu, most of the fluid originating from the slab was transported toward the mantle wedge tip through the weak hydrous layer, resulting in much less fluid being transported to the sub-arc mantle and narrow flux melting zone (Fig. 2d2).

Discussion

Our model demonstrated the formation of the cold nose via the downdip growth of the weak hydrous layer along the slab interface in both Kyushu and Shikoku/Chugoku. In the early stages of subduction, strong coupling is expected along the slab interface due to the small viscosity contrast between the hydrated forearc mantle and the surrounding mantle (Supplementary Figs. 5a and 6a). This promotes the formation of a hot forearc, consistent with the surface heat flow in the forearc (Supplementary Figs. 7a and 8a). As subduction progresses, a weak hydrous layer develops, and mechanical decoupling is facilitated by the increased viscosity contrast (Supplementary Figs. 5b and 6b), leading to the formation of a cold forearc mantle at ~ 12 Ma (Supplementary Figs. 7b and 8b). At present, the downdip extent of the weak hydrous layer is at a depth of ~ 90 km in both regions (Figs. 2c1 and 2c2). This is consistent with the presence of a cold nose observed in mature subduction zones worldwide[7] and the transition from strong mechanical coupling to decoupling occurring within the first 1–5 Ma since subduction initiation[33]. The depth range of serpentinite dehydration is comparable to the depths at which fluid-triggered instabilities occur along the subduction interface, as recorded in exhumed oceanic mantle

rocks[34]. Our results showed that the cold forearc is formed in both regions, regardless of the differences in the subduction parameters. This aligns with the low surface heat flow in the forearc observed in both regions (Supplementary Figs. 7 and 8), a characteristic commonly observed in subduction zones worldwide, indicating the presence of a cold nose[5–7].

Shear wave splitting in subduction zones serves as a proxy for the anisotropy structure of the forearc mantle and subducting slab. In SW Japan, where the contribution of anisotropy from the bending-related faults on the Philippine Sea Plate is minimal[35,36]the observed shear wave splitting parameters, characterized by trench-parallel fast directions and large delay times, are primarily controlled by the presence of the weak hydrous layer. The weak hydrous layer below the cold nose can cause trench-parallel fast direction and large delay times, both of which explain the seismic anisotropy observed in SW Japan[19,29] (Fig. 1).

While the presence of the weak hydrous layer was commonly observed in both Kyushu and Shikoku/Chugoku, the deep low-frequency tremors caused by the fluid migrating toward the mantle wedge corner through the weak hydrous layer were not observed in Kyushu. The variation in the dehydration behavior observed in the two regions may be due to the differences in the thermal structure of the slab and mantle wedge, which closely correlate with the age, dip, and convergence rate[13,14]. The slab age primarily controls the thermal structure of the slab itself, whereas the overall thermal state of a subduction zone (i.e., 'cold' vs. 'warm') reflects a combination of factors, including not only slab age but also convergence rate, slab dip, and thickness of the overriding plate[7,13,14,37]. Given the similar convergence rates and thickness of the overriding plate beneath the two regions, slab age and dip are likely the primary factors controlling the thermal state of the subduction zone and associated dehydration processes. Although slab dip affects the thermal structures of both the slab surface and the mantle wedge[7,38]the slab age exerts more dominant control[14]. In Kyushu, where the older plate subducts, most dehydration of the subducting slab occurred at depths greater than 100 km due to the cold slab temperature. As most of the fluid infiltrated the mantle wedge at sub-arc depths, only a small amount of fluid was transported along the weak hydrous layer and consequently did not reach the mantle wedge tip (Figs. 2d1 and 3a). This corresponds to the absence of deep low-frequency tremors in the forearc in Kyushu (Fig. 1). In contrast, the younger subducting slab beneath Shikoku/Chugoku dehydrated at the sub-forearc depths due to the warm slab, allowing most fluid to migrate through the weak hydrous layer and reach the mantle wedge tip (Figs. 2a2-2d2 and 3b). A large amount of fluid transport to the mantle wedge tip contributed to the frequent tremors observed in Shikoku/Chugoku (Fig. 1).

In the previous study by Lee and Kim[21]the spontaneous emergence of a weak hydrous layer and its downdip growth successfully explained the forearc-to-arc volcanic front migration in SW Japan. The downdip growth of the weak hydrous layer facilitated mechanical decoupling between the slab and overlying mantle, leading to a transition from a hot forearc developed in the early stages of subduction to a cold nose[21]. Our modeling results also align well with the volcanic front migration in Shikoku/Chugoku, the formation of forearc high-magnesium andesite (HMA) in the mid-Miocene (~ 15–12 Ma), and Quaternary arc adakites[22,39].

Our model also captured the characteristics of the volcanic history observed in Kyushu during the same period. In Kyushu, forearc HMA also occurred in ~ 17–12 Ma[ref.40], which can be attributed to the development of a hot forearc caused by the subduction of the young and hot Shikoku Basin lithosphere including a spreading mid-ocean ridge[22]. The model results also showed that, in the early stages of subduction (~ 14–12 Ma), a weak hydrous layer did not form at the sub-forearc slab interface, resulting in the development of a hot forearc due to strong coupling between the slab and overlying mantle (Supplementary Figs. 1 and 2). As subduction continued, a cold nose developed due to progressive mechanical decoupling as the weak hydrous layer was formed and extended downward (Supplementary Figs. 3 and 4). This transition from a hot to cold forearc corresponds to the cessation of forearc volcanism and the occurrence of rear-arc volcanism in SW Japan during 12–4 Ma[ref.22]. Unlike in Shikoku/Chugoku, HMA occurred around 7–5 Ma in Kyushu, which might be due to slab melting caused by additional heat from the upwelling asthenospheric mantle associated with opening of the Okinawa Trough[22,41]. Between 4 and 0 Ma, active volcanism resumed in the arc, and the adakitic magma formed by slab melting at depths of 95–100 km could potentially be diluted by the abundant basaltic magma in the mantle wedge which the adakitic magma passes through[42,43] (Figs. 2a2-2d2). As the depth limit of slab melting is ~ 100 km, no adakitic magma is formed beyond that depth[42]. Although our model did not consider additional heat sources during back-arc opening, integrating such a factor could provide a more accurate understanding of the volcanic history of SW Japan.

As we have numerically demonstrated using the case of SW Japan, considering the spatiotemporal along-trench variation in subduction parameters is essential to understand the uneven distribution of volcanic and seismic activities. The use of this modeling approach has good potential to decipher other subduction zones where significant along-trench variations in slab geometry are present. Although it was not considered in this study, a possible disruption in slab geometry (e.g., slab tear) beneath SW Japan[44–46] may have significantly influenced the regional thermal structure, contributing to the localized volcanic and seismic activities. The Aleutians are another example of the uneven distribution of geochemical signatures in arc volcanoes, with the melting of subducting oceanic basalts observed only in the western Aleutians[47]. Two-dimensional numerical models, which consider time-evolving subduction parameters and along-trench variations in slab geometry, successfully explained that slab melting is restricted to the western Aleutians[48]. Central America exhibits characteristic volcanic activities, ranging from the occurrence of adakitic magma in Ecuador to the volcanic gap in Central Chile[49,50]. Through numerical modeling, the evolution of flat subduction demonstrates how changes in slab dip and the resulting thermal structure can explain the episodic slab melting and the cessation of melt production[49,51]. The modeling approach suggested in this study could aid in a better understanding of volcanic and seismic activities in global subduction zones by implementing more realistic slab dehydration and fluid migration.

Summary

To clarify the uneven distribution of volcanic and seismic activities observed in SW Japan, we performed numerical modeling considering the spatiotemporal differences in slab age, convergence rate, and dip in Kyushu and Shikoku/Chugoku. Even though the differences in subduction parameters create different thermal regimes, we confirmed the formation of a weak hydrous layer along the slab interface from the wedge tip to sub-arc depth in both regions. In Kyushu, the colder and steeper subducting slab triggers dehydration mostly at sub-arc depths, resulting in the migration of a smaller volume of fluid toward the wedge tip. This explains the absence of deep low-frequency tremors in the forearc. Most fluid percolated into the sub-arc mantle wedge increases magma production, which explains the densely populated arc volcanoes in Kyushu. Adakitic magma formed at depths shallower than the depth limit of adakitic magmatism in Kyushu could be diluted by the abundant basaltic magma in the mantle wedge which the adakitic magma passes through. In Shikoku/Chugoku, the warmer and gentler subducting slab leads to a large volume of fluid transport at sub-forearc depth. Most of the fluid reaches the mantle wedge tip through the weak hydrous layer, generating frequent deep low-frequency tremors in the forearc. The smaller volume of fluid transport to the sub-arc mantle triggers less intense flux melting, resulting in sparse monogenic volcanism with adakitic magma. The spatiotemporal features of late Cenozoic arc volcanism in SW Japan can be well explained by the progressive downdip growth of the weak hydrous layer and the transition from a hot to cold forearc mantle during the early stages of subduction.

Methods

Governing equations

In our model, the mantle wedge flow is dynamically driven by a kinematically driven subducting slab with a predefined velocity and age. For the solid-state mantle flow, the incompressible Stokes and energy equations were solved for the mantle wedge, while only the energy equation was solved for the subducting plate and overlying continental crust:

continuity equation,

$$0 = \nabla \cdot \vec{V}_s \tag{1}$$

momentum equation,

$$0 = -\nabla P + \nabla \cdot (2\eta \dot{\epsilon}) \tag{2}$$

energy equation,

$$\rho_s C_p \left(\frac{\partial T}{\partial t} + \vec{V}_s \cdot \nabla \mathrm{T} \right) = \nabla \cdot (k \nabla \mathrm{T}) + \mathrm{H} \tag{3}$$

where $\vec{V}_s$ is the solid velocity, P is the dynamic pressure, η is the shear viscosity, $\dot{\epsilon}$ is the strain rate tensor, ρ_s is the solid (rock) density, C_p is the specific heat at constant pressure, T is the temperature, t is the time, k is the thermal conductivity, and H is the radiogenic heat production. Shear heating along the surface of the subducting slab is not considered, as it has a negligible effect on the thermal structure of the slab beneath the forearc mantle[38].

In this model, following Lee and Kim[21]the rheology of weak hydrous minerals (e.g., serpentine) was considered in viscosity calculations. We assumed that the serpentine and olivine represent the viscosity of serpentinite and mantle, respectively. The presence of serpentine under sub-forearc pressure and temperature conditions reduces viscosity by up to three orders of magnitude compared to that of olivine[52]. Further, fluid in this study is represented as water. As the amount of bound water increases, the viscosity of nominally anhydrous olivine decreases. Consequently, the viscosity of bound water-bearing olivine was approximated by multiplying the viscosity reduction factor, a function of the amount of bound water, by the calculated viscosities of diffusion and dislocation creep of dry olivine[53,54]. Taking into account all the rheologies, we used the composite viscosity of olivine and serpentine as follows:

composite viscosity,

$$\eta = \left(\frac{1}{\eta_{ol,\ dif}} + \frac{1}{\eta_{ol,dis}} + \frac{1}{\eta_{serp,dis}} \right)^{-1} \tag{4}$$

diffusion creep of olivine,

$$\eta_{ol,dif} = \left(\frac{\omega_r}{\omega} \right) \frac{\mu}{2A_{ol,dif}} \left(\frac{b}{d} \right)^{-m} exp \left(\frac{E_{ol,dif} + PV_{ol,dif}}{R(T + \bar{T})} \right) \tag{5}$$

dislocation creep of olivine,

$$\eta_{ol,dis} = \left(\frac{3\omega_r}{\omega + 2\omega_r} \right) \frac{\mu}{2} A_{ol,dis}^{-\frac{1}{n_{ol}}} exp \left(\frac{E_{ol,dis} + PV_{ol,dis}}{n_{ol} R(T + \bar{T})} \right) \dot{\epsilon}^{\frac{1-n_{ol}}{n_{ol}}} \tag{6}$$

dislocation creep of serpentine,

$$\eta_{serp,dis} = f(\omega)\frac{1}{2}A_{serp,dis}^{-\frac{1}{n_{serp}}} exp\left(\frac{E_{serp,dis}+PV_{serp,dis}}{n_{serp}R(T+\bar{T})}\right)\dot{\epsilon}^{\frac{1-n_{serp}}{n_{serp}}} \quad (7)$$

where *ol*, *serp*, *dif*, and *dis* represent olivine, serpentine, diffusion creep, and dislocation creep, respectively. ω is the mass fraction of bound water and ω_r is the background mass fraction of bound water for dry olivine. μ is the shear modulus, A is the pre-exponential factor, b is the Burgers vector, d is the grain size, m is the grain size exponent, n is the stress exponent, E and V are the activation energy and volume, respectively. R is the gas constant, $f(\omega)$ is a function of bound water that activates serpentine viscosity and reaches unity when 20% or more of the peridotite is serpentinized (ω : 2.153 wt%). When the amount of bound water is small (ω < 0.15 wt%), the mantle viscosity is primarily controlled by the olivine viscosity, reduced by the increased bound water[54,55]. At higher bound water levels (ω > 2.153 wt%), the serpentine viscosity dominates. This rheological configuration leads to significantly low viscosity in the sub-forearc mantle where hydrous minerals are present.

The bound water in hydrous minerals is transported along with the solid flow in the slab and mantle wedge, while the free water in pores is carried by porous flow within the deforming solid. By applying the zero-compaction length and small-porosity approximations, the transport of bound and free water can be calculated as follows[12,56–59]:

Bound-water transport,

$$\frac{\partial\omega}{\partial t} + \nabla\cdot\left(\vec{V}_s\omega\right) = \Gamma_{f\to s}/\rho_s + \nabla\cdot(\kappa_\omega\nabla\omega) \quad (8)$$

$$\frac{\partial\psi}{\partial t} + \nabla\cdot(\vec{V}_f\psi) = \Gamma_{s\to f}/\rho_f + \nabla\cdot(\kappa_\psi\nabla\psi) \quad (9)$$

.

where $\Gamma_{f\to s}$ and $\Gamma_{s\to f}$ are the rates of mass transfer by hydration and dehydration, respectively. ρ_s and ρ_f are the solid density and free-water density, respectively. κ_ω and κ_ψ are the artificial diffusivities of bound and free water for model stability, respectively. ψ is the volume fraction of free water (i.e., porosity). The free-water velocity, $\vec{V}_f$, is assumed to be controlled by the solid flow and fluid buoyancy and can be calculated as follows[12,57]:

$$\vec{V}_f = \vec{V}_s - \frac{\mathbf{K}}{\eta_f\psi}(\nabla P - \triangle\rho)\vec{g} \quad (10)$$

where $\mathbf{K}$ is the permeability tensor ($\mathbf{K_{ij}}$, i and j for the x- and y-axes, respectively). η_f is the free water viscosity, $\triangle\rho$ is the density difference between the solid and free water ($\rho_s - \rho_f$), and g is the gravitational acceleration. The effect of dynamic pressure on free-water transport is neglected in this study, as the previous work by Lee and Kim[21] demonstrated consistent free-water transport and spatiotemporal formation of a weak hydrous layer, regardless of dynamic pressure.

Serpentine foliation formed parallel to the slab interface serves as a pathway for free-water transport toward the mantle wedge tip[60]. The permeability along the serpentine foliation is about two orders of magnitude greater than in the direction perpendicular to the foliation, yet it remains lower than the isotropic permeability of peridotite[60]. The permeability tensor of serpentinite can be expressed as a function of the foliation orientation (θ) parallel to the slab geometry from the reference frame (x-axis) as follows[61]:

Permeability tensor of serpentinite,

$$\mathbf{K} = \begin{pmatrix} K_n sin^2\theta + K_p cos^2\theta & (K_n - K_p)sin\theta\, cos\theta \\ (K_n - K_p)sin\theta\, cos\theta & K_n cos^2\theta + K_p sin^2\theta \end{pmatrix} \quad (11)$$

.

where K_n and K_p are the permeabilities normal and parallel to the foliation, defined as 0.0016 K_r and 0.08 K_r, respectively. The isotropic peridotite permeability (K_r) is approximated as that of a texturally equilibrated rock[62]:

$$K_r = \frac{d^2\psi^3}{C_d} \quad (12)$$

.

where C_d is the geometrical factor. A reference permeability (K_0) is obtained from a background volume fraction of free water ($\psi_0 = 10^{-4}$) and a volume fraction of 10^{-3}. The permeability anisotropy of the serpentinite channel was assumed to be activated when 20% of the peridotite was serpentinized[63]. The permeability values calculated in our models range from 10^{-14} to $10^{-20} m^2$, consistent with previous experimental estimates[64–66].

The (de)hydration of the oceanic crust and mantle was addressed using a simplified kinetic relationship, formulated as follows[58,59]:

Mass transfer from free to bound water,

$$\Gamma_{f\to s} = \frac{\rho_s \left|\vec{V}_s\right| \left(\omega_{max\left(P,T+\bar{T}\right)} - \omega_{\left(P,T+\bar{T}\right)}\right)}{l} \tag{13}$$

Mass transfer from bound water to free water,

$$\Gamma_{s\to t} = -\Gamma_{f\to s} \tag{14}$$

where $\left|\vec{V}_s\right|$ is the magnitude of the solid velocity. $\omega_{max\left(P,T+\bar{T}\right)}$ is the maximum mass fraction (solubility) of bound water at a given pressure and temperature. $\omega_{\left(P,T+\bar{T}\right)}$ is the mass fraction of bound water, and l is the (de)hydration length, short enough for rapid (de)hydration without creating a metastable phase. The parameter values used in this study are listed in Supplementary Table 1.

Model setup

To consider the variation of subduction parameters along SW Japan, we set the model geometries from the trench-normal profiles crossing Kyushu and Shikoku/Chugoku (Fig. 1 and Supplementary Fig. 10). Both models consisted of subducting slabs and overlying continental crust with thicknesses of 100 km and 32.5 km, respectively (Supplementary Fig. 10). The geometries and boundary conditions used in the numerical models are presented in Supplementary Fig. 10. The predefined convergence rate was assigned along the slab interface for solving the Stokes equation in the mantle wedge. No prescribed decoupling zone was imposed along the slab interface except for the tip. At the slab interface near the tip, we set a 1-km-long linear velocity ramp to minimize the pressure singularity[67]. No-slip and open boundaries were set for the continental Moho and outer boundary of the mantle wedge, respectively. The initial velocity of the mantle wedge was set to zero. To solve the energy equation, the surface temperature of the continental crust was set to 0 °C. The bottom of the subducting slab was insulated while the horizontal boundary of the subducting slab at a depth of 125 km was prescribed as an open boundary. The half-space cooling model for a 40-Myr plate was calculated using a mantle potential temperature of 1350 °C. The calculated temperature profile was prescribed to the backarc-side vertical boundary of the mantle wedge at a depth of 100 km. To consider subduction history, the time-evolving convergence rate and age of the subducting slab are assigned to the slab geometry and trench-side vertical boundary, respectively[17,24,68] (Supplementary Fig. 11). Thus, the half-space cooling model prescribed on the trench-side vertical boundary is updated with subduction history. The mantle adiabatic temperature (0.35 K km^{-1}) was added to the calculated temperature as a posterior.

We divided the hydrated portion of the slab into three layers[12,21]: a 1-km-thick basaltic oceanic crust, a 5-km-thick gabbroic oceanic crust layer, and a 5-km-thick residual harzburgite layer (Supplementary Fig. 10). The sedimentary layer was excluded from consideration due to its minimal thickness (~0.3 km) being subducted into the mantle[13]which contributed negligibly to the bound-water budget. The relevant phase diagrams showing the water solubilities of each layer were evaluated using the Perple_X software[69] and presented in Supplementary Fig. 12.

The governing equations with the defined rheologies and water solubilities are simultaneously calculated using the commercial finite element package COMSOL Multiphysics®. The model domain was discretized into unstructured triangular elements. To enhance accuracy, finer elements, with sizes of approximately 0.6 km and 0.2 km, were predominantly used for the hydrated portions of the subducting slab and the base of the mantle wedge, respectively. The fully coupled PARDISO solver was used with the generalized alpha method for time stepping.

Data availability

Data used in this study can be found in the published literatures and cited references. All numerical model results used in this study are available on an open repository, Zenodo (https://zenodo.org/records/14788420).

Received: 2 February 2025; Accepted: 1 July 2025
Published online: 12 July 2025

References

1. Gill, J. *Orogenic Andesites and Plate Tectonics*309 (pp (Springer Science, 1981).
2. Grove, T. L., Chatterjee, N., Parman, S. W. & Médard, E. The influence of H2O on mantle wedge melting. *Earth Planet. Sci. Lett.* **249**, 74–89. https://doi.org/10.1016/j.epsl.2006.06.043 (2006).
3. Morris, P. A. Slab melting as an explanation of quaternary volcanism and aseismicity in Southwest Japan. *Geology* **23**, 395–398 (1995).
4. Zellmer, G. F., Iizuka, Y., Miyoshi, M., Tamura, Y. & Tatsumi, Y. Lower crustal H2O controls on the formation of Adakitic melts. *Geology* **40**, 487–490. https://doi.org/10.1130/G32912.1 (2012).
5. Hyndman, R. D. & Peacock, S. M. Serpentinization of the forearc mantle. *Earth Planet. Sci. Lett.* **212**, 417–432. https://doi.org/10.1016/S0012-821X(03)00263-2 (2003).
6. Currie, C. A. & Hyndman, R. D. The thermal structure of subduction zone back arcs. *J. Geophys. Res. Solid Earth*. **111** https://doi.org/10.1029/2005JB004024 (2006).
7. Wada, I. & Wang, K. Common depth of slab-mantle decoupling: reconciling diversity and uniformity of subduction zones. *Geochem. Geophys. Geosyst.* **10** https://doi.org/10.1029/2009gc002570 (2009).
8. Saffer, D. M. & Tobin, H. J. Hydrogeology and mechanics of subduction zone forearcs: fluid flow and pore pressure. *Annu. Rev. Earth Planet. Sci.* **39**, 157–186. https://doi.org/10.1146/annurev-earth-040610-133408 (2011).

9. Obara, K. Nonvolcanic deep tremor associated with subduction in Southwest Japan. *Science* **296**, 1679–1681. https://doi.org/10.1126/science.1070378 (2002).
10. Katsumata, A. & Kamaya, N. Low-frequency continuous tremor around the Moho discontinuity away from volcanoes in the Southwest Japan. *Geophys. Res. Lett.* **30** https://doi.org/10.1029/2002GRL015981 (2003). 20 – 1.
11. Katayama, I., Terada, T., Okazaki, K. & Tanikawa, W. Episodic tremor and slow slip potentially linked to permeability contrasts at the Moho. *Nat. Geosci.* **5**, 731–734. https://doi.org/10.1038/ngeo1559 (2012).
12. Lee, C. & Kim, Y. Role of warm subduction in the seismological properties of the forearc mantle: an example from Southwest Japan. *Sci. Adv.* **7**, eabf8934. https://doi.org/10.1126/sciadv.abf8934 (2021).
13. van Keken, P. E., Hacker, B. R., Syracuse, E. M. & Abers, G. A. Subduction factory: 4. Depth-dependent flux of H2O from subducting slabs worldwide. *J. Geophys. Res. Solid Earth*. **116** https://doi.org/10.1029/2010jb007922 (2011).
14. Syracuse, E. M., van Keken, P. E. & Abers, G. A. The global range of subduction zone thermal models. *Phys. Earth Planet. Inter*. **183**, 73–90. https://doi.org/10.1016/j.pepi.2010.02.004 (2010).
15. Otofuji, Y. I., Matsuda, T. & Nohda, S. Paleomagnetic evidence for the miocene counter-clockwise rotation of Northeast Japan-rifting process of the Japan Arc. *Earth Planet. Sci. Lett.* **75**, 265–277. https://doi.org/10.1016/0012-821X(85)90108-6 (1985).
16. Okino, K., Ohara, Y., Kasuga, S. & Kato, Y. The Philippine sea: new survey results reveal the structure and the history of the marginal basins. *Geophys. Res. Lett.* **26**, 2287–2290. https://doi.org/10.1029/1999GL900537 (1999).
17. Tatsumi, Y., Suenaga, N., Yoshioka, S., Kaneko, K. & Matsumoto, T. Contrasting volcano spacing along SW Japan Arc caused by difference in age of subducting lithosphere. *Sci. Rep.* **10**, 15005. https://doi.org/10.1038/s41598-020-72173-6 (2020).
18. Salah, M. K., Seno, T. & Iidaka, T. Upper mantle anisotropy beneath central and Southwest japan: an insight into subduction-induced mantle flow. *J. Geodyn.* **46**, 21–37. https://doi.org/10.1016/j.jog.2008.04.002 (2008).
19. Wirth, E. & Long, M. D. Frequency-dependent shear wave splitting beneath the Japan and Izu-Bonin subduction zones. *Phys. Earth Planet. Interiors*. **181**, 141–154. https://doi.org/10.1016/j.pepi.2010.05.006 (2010).
20. Suenaga, N. et al. Two-dimensional thermal modeling of the Philippine sea plate subduction in central japan: implications for gap of low-frequency earthquakes and tectonic tremors. *J. Geophys. Res. Solid Earth*. **124**, 6848–6865. https://doi.org/10.1029/2018JB017068 (2019).
21. Lee, C. & Kim, Y. Understanding subduction infancy to mature subduction in Southwest Japan via the self-consistent formation of a weak slab interface. *Sci. Rep.* **13**, 21425. https://doi.org/10.1038/s41598-023-48746-6 (2023).
22. Kimura, J. I., Stern, R. J. & Yoshida, T. Reinitiation of subduction and magmatic responses in SW Japan during neogene time. *Geol. Soc. Am. Bull.* **117**, 969–986. https://doi.org/10.1130/b25565.1 (2005).
23. Bird, P. An updated digital model of plate boundaries. *Geochem. Geophys. Geosyst.* **4** https://doi.org/10.1029/2001GC000252 (2003).
24. Miyazaki, K., Nakajima, J., Suenaga, N. & Yoshioka, S. Deep subduction of the Philippine sea slab and formation of slab window beneath central Japan. *Earth Planet Space*. **75**, 93. https://doi.org/10.1186/s40623-023-01846-z (2023).
25. Maeda, T. & Obara, K. Spatiotemporal distribution of seismic energy radiation from low-frequency tremor in Western Shikoku. *Japan J Geophys. Res. Solid Earth*. **114** https://doi.org/10.1029/2008JB006043 (2009).
26. Obara, K., Tanaka, S., Maeda, T. & Matsuzawa, T. Depth-dependent activity of non-volcanic tremor in Southwest Japan. *Geophys. Res. Lett.* **37** https://doi.org/10.1029/2010GL043679 (2010).
27. Kano, M. et al. Development of a slow earthquake database. *Seismol. Res. Lett.* **89**, 1566–1575. https://doi.org/10.1785/0220180021 (2018).
28. National Research Institute for Earth Science and Disaster Resilience. Activity of deep low-frequency tremor in Southwest Japan (November, 2020 - April, 2021). *Rep. Coordinating Comm. Earthq. Prediction*. **106**, 463–467 (2021).
29. Long, M. D. & van der Hilst, R. D. Upper mantle anisotropy beneath Japan from shear wave splitting. *Phys. Earth Planet. Interiors*. **151**, 206–222. https://doi.org/10.1016/j.pepi.2005.03.003 (2005).
30. Kelley, K. A. et al. Mantle melting as a function of water content beneath the Mariana Arc. *J. Petrol.* **51**, 1711–1738. https://doi.org/10.1093/petrology/egq036 (2010).
31. Schmidt, M. W. & Poli, S. Experimentally based water budgets for dehydrating slabs and consequences for Arc magma generation. *Earth Planet. Sci. Lett.* **163**, 361–379. https://doi.org/10.1016/S0012-821X(98)00142-3 (1998).
32. Walowski, K. J., Wallace, P. J., Hauri, E. H., Wada, I. & Clynne, M. A. Slab melting beneath the cascade Arc driven by dehydration of altered oceanic peridotite. *Nat. Geosci.* **8**, 404–408. https://doi.org/10.1038/ngeo2417 (2015).
33. Agard, P. et al. The subduction plate interface: rock record and mechanical coupling (from long to short timescales). *Lithos* **320**, 537–566. https://doi.org/10.1016/j.lithos.2018.09.029 (2018).
34. Muñoz-Montecinos, J. et al. Fluid-driven shear instabilities in the subducted oceanic mantle at intermediate depths: insights from Western alps meta-ophiolites. *Geochem. Geophys. Geosyst.* **25**, e2024GC011581. https://doi.org/10.1029/2024GC011581 (2024).
35. Kodaira, S. et al. Western Nankai trough seismogenic zone: results from a wide-angle ocean bottom seismic survey. *J. Geophys. Res. Solid Earth*. **105**, 5887–5905. https://doi.org/10.1029/1999JB900394 (2000).
36. Faccenda, M., Burlini, L., Gerya, T. V. & Mainprice, D. Fault-induced seismic anisotropy by hydration in subducting oceanic plates. *Nature* **455**, 1097–1100. https://doi.org/10.1038/nature07376 (2008).
37. Liu, M. Q., Li, Z. H. & Yang, S. H. Diapir versus along-channel ascent of crustal material during plate convergence: constrained by the thermal structure of subduction zones. *J. Asian Earth Sci.* **145**, 16–36. https://doi.org/10.1016/j.jseaes.2017.02.036 (2017).
38. Lee, C. & King, S. D. Effect of mantle compressibility on the thermal and flow structures of the subduction zones. *Geochem. Geophys. Geosyst.* **10** https://doi.org/10.1029/2008GC002151 (2009).
39. Tatsumi, Y. et al. Tectonic setting of high-Mg andesite magmatism in the SW Japan arc: K–Ar chronology of the Setouchi volcanic belt. *Geophys. J. Int.* **144**, 625–631. https://doi.org/10.1046/j.1365-246x.2001.01358.x (2001).
40. Tatsumi, Y. et al. The petrology and geochemistry of high-magnesium andesites at the Western tip of the Setouchi volcanic belt, SW Japan. *J. Petrol.* **44**, 1561–1578. https://doi.org/10.1093/petrology/egg049 (2003).
41. Shinjo, R., Chung, S. L., Kato, Y. & Kimura, M. Geochemical and Sr-Nd isotopic characteristics of volcanic rocks from the Okinawa trough and Ryukyu Arc: implications for the evolution of a young, intracontinental back Arc basin. *J. Geophys. Res. Solid Earth*. **104**, 10591–10608. https://doi.org/10.1029/1999JB900040 (1999).
42. Mibe, K. et al. Slab melting versus slab dehydration in subduction-zone magmatism. *Proc. Natl. Acad. Sci.* **108**, 8177–8182. https://doi.org/10.1073/pnas.1010968108 (2011).
43. Yogodzinski, G. M. & Kelemen, P. B. Slab melting in the aleutians: implications of an ion probe study of clinopyroxene in primitive Adakite and basalt. *Earth Planet. Sci. Lett.* **158**, 53–65. https://doi.org/10.1016/S0012-821X(98)00041-7 (1998).
44. Cao, L., Wang, Z., Wu, S. & Gao, X. A new model of slab tear of the subducting Philippine sea plate associated with Kyushu-Palau-Ridge subduction. *Tectonophysics* **636**, 158–169. https://doi.org/10.1016/j.tecto.2014.08.012 (2014).
45. Pineda-Velasco, I., Kitagawa, H., Nguyen, T. T., Kobayashi, K. & Nakamura, E. Production of high-Sr andesite and dacite magmas by melting of subducting oceanic lithosphere at propagating slab tears. *J. Geophys. Res. Solid Earth*. **123**, 3698–3728. https://doi.org/10.1029/2017JB015066 (2017).
46. Sun, M., Yu, Y., Gao, S. S. & Liu, K. H. Stagnation and tearing of the subducting Northwest Pacific slab. *Geology* **50**, 676–680. https://doi.org/10.1130/G49862.1 (2022).
47. Kelemen, P. B., Yogodzinski, G. M. & Scholl, D. W. Along-strike variation in the Aleutian Island arc: genesis of high mg# andesite and implications for continental crust. *Inside Subduction Fact.* **138**, 223–276. https://doi.org/10.1029/138GM11 (2003).

48. Lee, C. & King, S. D. Why are high-Mg# andesites widespread in the Western aleutians?? A numerical model approach. *Geology* **38**, 583–586. https://doi.org/10.1130/G30714.1 (2010).
49. Gutscher, M. A., Maury, R., Eissen, J. P. & Bourdon, E. Can slab melting be caused by flat subduction?. *Geology* **28**, 535–538 (2000).
50. Beate, B. et al. Mio–Pliocene Adakite generation related to flat subduction in Southern ecuador: the Quimsacocha volcanic center. *Earth Planet. Sci. Lett.* **192**, 561–570. https://doi.org/10.1016/S0012-821X(01)00466-6 (2001).
51. Gauthier, A., Larvet, T., Le Pourhiet, L. & Moretti, I. Water budget in flat vs. steep subduction: implication for volcanism and potential for H_2 production. *BSGF-Earth Sci. Bull.* **195**, 26. https://doi.org/10.1051/bsgf/2024026 (2024).
52. Hilairet, N. et al. High-Pressure creep of serpentine, interseismic deformation, and initiation of subduction. *Science* **318**, 1910–1913. https://doi.org/10.1126/science.1148494 (2007).
53. Karato, S. I. & Wu, P. Rheology of the upper mantle: a synthesis. *Science* **260**, 771–778. https://doi.org/10.1126/science.260.5109.771 (1993).
54. Richard, G. C. & Iwamori, H. Stagnant slab, wet plumes and cenozoic volcanism in East Asia. *Phys. Earth Planet. Inter.* **183**, 280–287. https://doi.org/10.1016/j.pepi.2010.02.009 (2010).
55. Angel, R. J. Equations of state. In Hazen, R.M., Downs, R. T. (Eds.), High-pressure, high-temperature crystal chemistry. *Rev. Mineral. Geochem.* 41, 35–60 (2001).
56. Wada, I. & Behn, M. D. Focusing of upward fluid migration beneath volcanic arcs: effect of mineral grain size variation in the mantle wedge. *Geochem. Geophys. Geosyst.* **16**, 3905–3923. https://doi.org/10.1002/2015GC005950 (2015).
57. Morishige, M. & van Keken, P. E. Along-arc variation in short-term slow slip events caused by 3-D fluid migration in subduction zones. *J. Geophys. Res. Solid Earth*. **122**, 1434–1448. https://doi.org/10.1002/2016JB013091 (2017).
58. Yoo, S. & Lee, C. Correlation of quaternary volcano clusters with partial melting of mantle wedge, Northeast japan: A numerical model study. *Geophys. Res. Lett.* **47** https://doi.org/10.1029/2019gl086205 (2020).
59. Lee, C., Seoung, D. & Cerpa, N. G. Effect of water solubilities on dehydration and hydration in subduction zones and water transport to the deep mantle: implications for natural subduction zones. *Gondwana Res.* **89**, 287–305. https://doi.org/10.1016/j.gr.2020.10.012 (2021).
60. Kawano, S., Katayama, I. & Okazaki, K. Permeability anisotropy of serpentinite and fluid pathways in a subduction zone. *Geology* **39**, 939–942. https://doi.org/10.1130/g32173.1 (2011).
61. Taylor-West, J. & Katz, R. F. Melt-preferred orientation, anisotropic permeability and melt-band formation in a deforming, partially molten aggregate. *Geophys. J. Int.* **203**, 1253–1262. https://doi.org/10.1093/gji/ggv372 (2015).
62. Wark, D. A., Williams, C. A., Watson, E. B. & Price, J. D. Reassessment of pore shapes in microstructurally equilibrated rocks, with implications for permeability of the upper mantle. *J. Geophys. Res. Solid Earth*. **108** https://doi.org/10.1029/2001jb001575 (2003).
63. Escartín, J., Hirth, G. & Evans, B. Strength of slightly serpentinized peridotites: implications for the tectonics of oceanic lithosphere. *Geology* **29**, 1023–1026 (2001).
64. Skarbek, R. M. & Saffer, D. M. Pore pressure development beneath the décollement at the Nankai subduction zone: implications for plate boundary fault strength and sediment dewatering. *J. Geophys. Res. Solid Earth*. **114** https://doi.org/10.1029/2008JB006205 (2009).
65. Takahashi, M., Azuma, S., Uehara, S. I., Kanagawa, K. & Inoue, A. Contrasting hydrological and mechanical properties of clayey and silty muds cored from the shallow Nankai trough accretionary Prism. *Tectonophysics* **600**, 63–74. https://doi.org/10.1016/j.tecto.2013.01.008 (2013).
66. Muñoz-Montecinos, J. & Behr, W. M. Transient permeability of a deep-seated subduction interface shear zone. *Geophys. Res. Lett.* **50** (20). https://doi.org/10.1029/2023GL104244 (2023). e2023GL104244.
67. van Keken, P. E. et al. A community benchmark for subduction zone modeling. *Phys. Earth Planet. Inter.* **171**, 187–197. https://doi.org/10.1016/j.pepi.2008.04.015 (2008).
68. Seno, T., Stein, S. & Gripp, A. E. A model for the motion of the Philippine sea plate consistent with NUVEL-1 and geological data. *J. Geophys. Res. Solid Earth*. **98**, 17941–17948. https://doi.org/10.1029/93JB00782 (1993).
69. Connolly, J. A. D. Computation of phase equilibria by linear programming: A tool for geodynamic modeling and its application to subduction zone decarbonation. *Earth Planet. Sci. Lett.* **236**, 524–541. https://doi.org/10.1016/j.epsl.2005.04.033 (2005).

Acknowledgements

The authors appreciate the insightful comments and suggestions provided by the three anonymous reviewers, which have helped improve the quality of this manuscript. This study is funded by the National Research Foundation of Korea Grant RS-2022-NR070842 to G. H. and Y.K. and Grant RS-2025-00514972 to C.L.

Author contributions

G. H., C.L. and Y.K conceived the study. C.L. performed the numerical experiments. G.H. analyzed the data. G.H., C.L., and Y.K. wrote the manuscript.

Declarations

Competing interests

The authors declare no competing interests.

Additional information

Supplementary Information The online version contains supplementary material available at https://doi.org/10.1038/s41598-025-10026-w.

Correspondence and requests for materials should be addressed to C.L. or Y.K.